

A TURBINE RESEARCH FACILITY TO STUDY TIP DESENSITIZATION INCLUDING COOLING FLOWS

Cengiz Camci

Department of Aerospace Engineering
Turbomachinery Heat Transfer Laboratory
The Pennsylvania State University
University Park, PA 16802
cxc11@psu.edu
<http://www.personal.psu.edu/cxc11/>

Abstract

This paper deals with the description of the Axial Flow Turbine Research Facility (AFTRF) installed at the Turbomachinery Laboratory of the Pennsylvania State University. The AFTRF is a single-stage cold flow turbine specifically designed for studying unsteady/turbulent viscous flow details of three-dimensional passage flows. The facility diameter is 91.66 cm (3 feet) and the hub-to-tip ratio of the blading is 0.73. 23 nozzle vanes and 29 rotor blades followed by outlet guide vanes. The blading design embodies modern HP turbine design philosophy, loading and flow coefficient, reaction, aspect ratio, and blade turning angles, all within current aircraft engine design turbine practice. State-of-the-art quasi-3D blade design techniques were used to design the vane and the blade shapes. The vanes and blades are heavily instrumented with fast response pressure, shear stress, and velocity probes and have provision for flow visualization and laser Doppler anemometer measurement. Furthermore, provision has been made, for detailed nozzle wake, rotor wake and boundary layer surveys. A 150 channel slip ring unit is used for transmitting the rotor data to a stationary instrumentation system. The recent modifications to the cold flow turbine AFTRF include an intra-stage coolant injection system, a stationary-to-rotating air transfer system and a blade tip cooling system. The implementation of a stereoscopic Particle Image Velocimetry (PIV) system in the rotor frame of reference is under progress. The most recent studies include the installation of tip desensitization geometries such as “tip platform extensions”, “squealer rim arrangements” and “tip cooling schemes” for tip leakage reduction. This document is an updated version of the original AFTRF design papers presented in [1],[2].

INTRODUCTION

The present knowledge of turbine flow field, especially the rotor flow field, is inadequate. The flow field is three-dimensional and unsteady, with the presence of laminar, transitional and turbulent regions near the blade surface. Some of the three-dimensional effects present are compressibility, radially varying thickness, annulus wall area changes and flaring, radially varying enthalpy, radial component of blade force, radially varying blade heat transfer, non-uniform entry flow and temperature field, and leakage and secondary flows. The three-dimensional viscous flows and turbulence effects are mainly caused by the three-dimensional boundary layers on blades and wakes, annulus wall and hub wall boundary layers including tip leakage flows, shock/boundary layer interaction, and secondary flows in annulus wall and hub wall boundary layers. The presence of horseshoe vortex near the blade leading edge, combined with thick blades and rapidly varying flow path and turning, makes the flow field truly complex. There are many other basic problems related to

turbines that remain unresolved. These are the vane-blade interaction and its effect on the unsteady pressure, unsteady heat transfer and flow induced vibration.

The objective of the research currently carried out in this facility is to gain a better understanding of the steady and unsteady flow field in a turbine stage. A 91.66 cm diameter Axial Flow Turbine Research Facility which simulates flow in a HP turbine has been designed, fabricated and installed at the Turbomachinery Laboratory in early nineties. The experimental results usually aid the physical understanding of complex flows and support the analytical and the computational code development. An additional objective is to generate benchmark quality data for the validation of three-dimensional Navier-Stokes codes and turbulence models for complex flows.

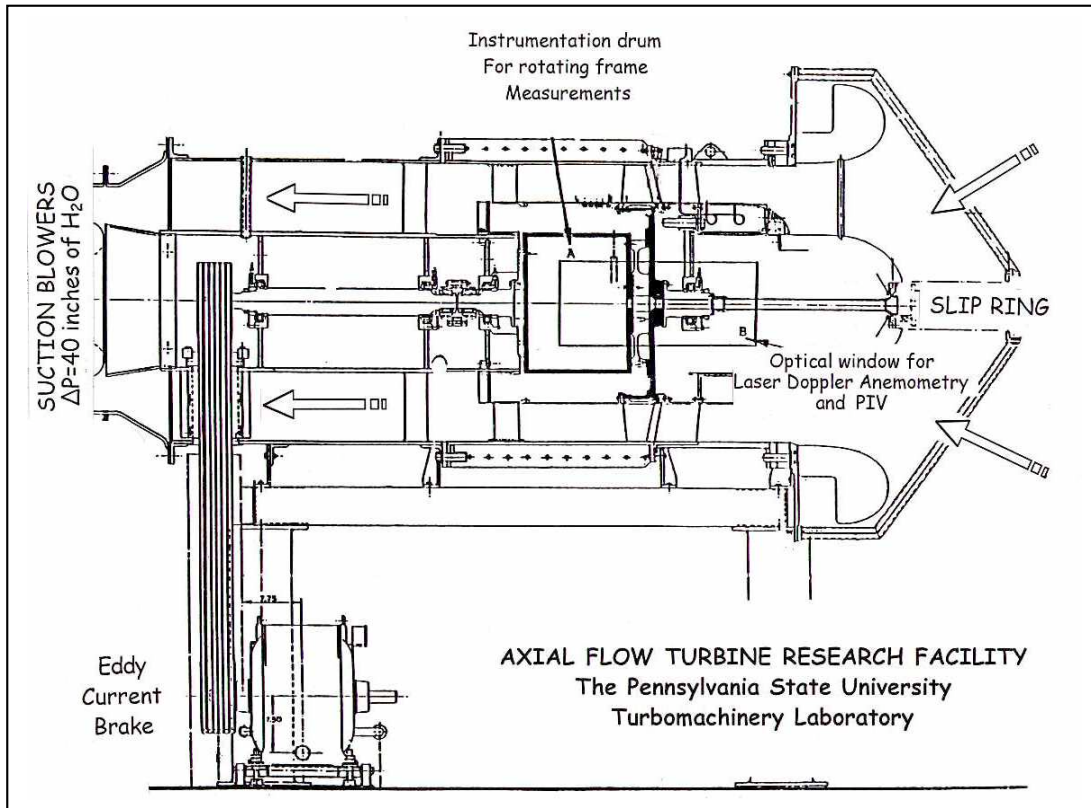


Figure 1. Large-scale cold flow turbine facility AFTRF

The large size of the rig shown in Figure 1 has the advantage of operating at Reynolds numbers representative of the engine environment. This allows duplication of Reynolds number sensitive fluid flow characteristics, such as wakes and boundary layers. The purpose of this paper is to present a description of the facility, instrumentation and the performance. The final section of the paper include the most recent modifications to the facility in the area of intra-stage coolant injection, stationary-to-rotating air transfer system and blade tip cooling system. A brief explanation of the new stereoscopic PIV system is also presented.

MAJOR CHARACTERISTICS OF THE TURBINE FACILITY

The Axial Flow Turbine Research Facility of The Pennsylvania State University is an open circuit facility 91.66 cm (3 feet) in diameter and a hub to tip radius ratio of 0.73, with an advanced

axial turbine blading configuration. The facility consists of a large bell-mouth inlet, an optional turbulence generating grid section, followed by a test section with a nozzle vane row and a rotor as shown in Figure 1. There are 23 nozzle guide vanes and 29 rotor blades followed by a set of outlet guide vanes. Provisions exist for changing the vane-blade axial spacing from 20 to 50 percent of chord. The bell-mouth inlet is housed in an enclosure (not shown) covered with wire mesh and a thin layer of rubber foam to filter the air prior to entry to the inlet.

A variable through-flow is provided by two auxiliary, adjustable pitch, axial flow fans and an aerodynamically designed throttle. The two fans in series produce a pressure rise of 74.7 mm Hg (30" of water) with a volumetric flow of 10.4 m^3 per second under nominal operating conditions. The power generated by the experimental turbine rotor assembly is absorbed by an eddy-current brake which is capable of absorbing up to 60.6 kw (90 Hp). The speed of the rotor can be varied between 175 and 1695 RPM with an Eddy-current-brake and can be held constant to ± 1 RPM, with normal fluctuations in line voltage. The eddy current brake is cooled by a closed loop chilled water cooling system.

The rotor and nozzle vane passages are instrumented with fast response instrumentation to measure steady (time averaged) and unsteady pressures and wall shear stresses. The details of the instrumentation used on the nozzle vane, rotor blade, nozzle casing, rotor hub, and nozzle hub will be described in a later section. Provision has been made for a laser window for LDV (Laser Doppler Velocimeter) measurement of the flow field upstream of the nozzle, nozzle passage, spacing between the rotor and the nozzle, rotor passage, and downstream of the rotor passage.

The facility is equipped with a rotating probe traversing mechanism. The traverse unit is mounted directly behind the rotor disk and has provisions for the radial and circumferential traverses in the rotating frame. The rotating-to-stationary data transmission system, attached to the rotor shaft ahead of the nose cone, is an integral part of the facility. It consists of a 150 ring mechanical (brush/coin type) slip ring unit, and a specialized ten-channel low noise/signal ratio mercury slip ring unit. A 32 channel electronic pressure scanner unit is located in the rotating drum downstream of the turbine rotor. The electrical signals carrying the pressure information is carried to the stationary frame through the slip ring assembly. The rotor frequency is accurately determined by using an optical encoder mounted on the turbine shaft.

A completely automated data processing system is built around a desktop computer. All of the data from both stationary and rotating instrumentation can be processed on-line. One of the long range goals of the turbine research is to acquire steady/unsteady heat transfer and aerodynamics data simultaneously.

BLADING AND FLOW PATH DESIGN

The principal aerodynamic and geometric design features of the nozzle vane and rotor blades are presented in this section. The aerodynamic design does embody modern turbine design philosophy. Stage loading flow coefficient, reaction, aspect ratios, and blade turning angles are all within the ranges of current design practice. State-of-the art quasi-3D design methods with empirical correlations for viscous losses were used to design the airfoil shapes. It is felt that the design is fully capable of meeting the intended research applications.

At the inception of the design the objective was that, where possible, the blading should be representative, both geometrically and aerodynamically, of a state-of-the-art HP turbine. When the blade design effort started, a comprehensive mechanical design for the rig was already in existence. As a result of this, and of the requirement to minimize any additional costs, the radius ratio and blade numbers were fixed. Additional restraints were placed on the blading design by the power available for

the through-flow air supply in the test facility. The requirement was for a blading design using modern techniques, based on typical recent technology.

DESIGN APPROACH

In order to ascertain how the design target might be met, a parametric one-dimensional mean line study was made. This was combined with a free-vortex distribution to attain radial equilibrium and used a turbine performance model from the open literature to account for real flow effects in the turbomachinery. The optimized mean-line solution is characterized broadly by the parameters shown in Table 1.

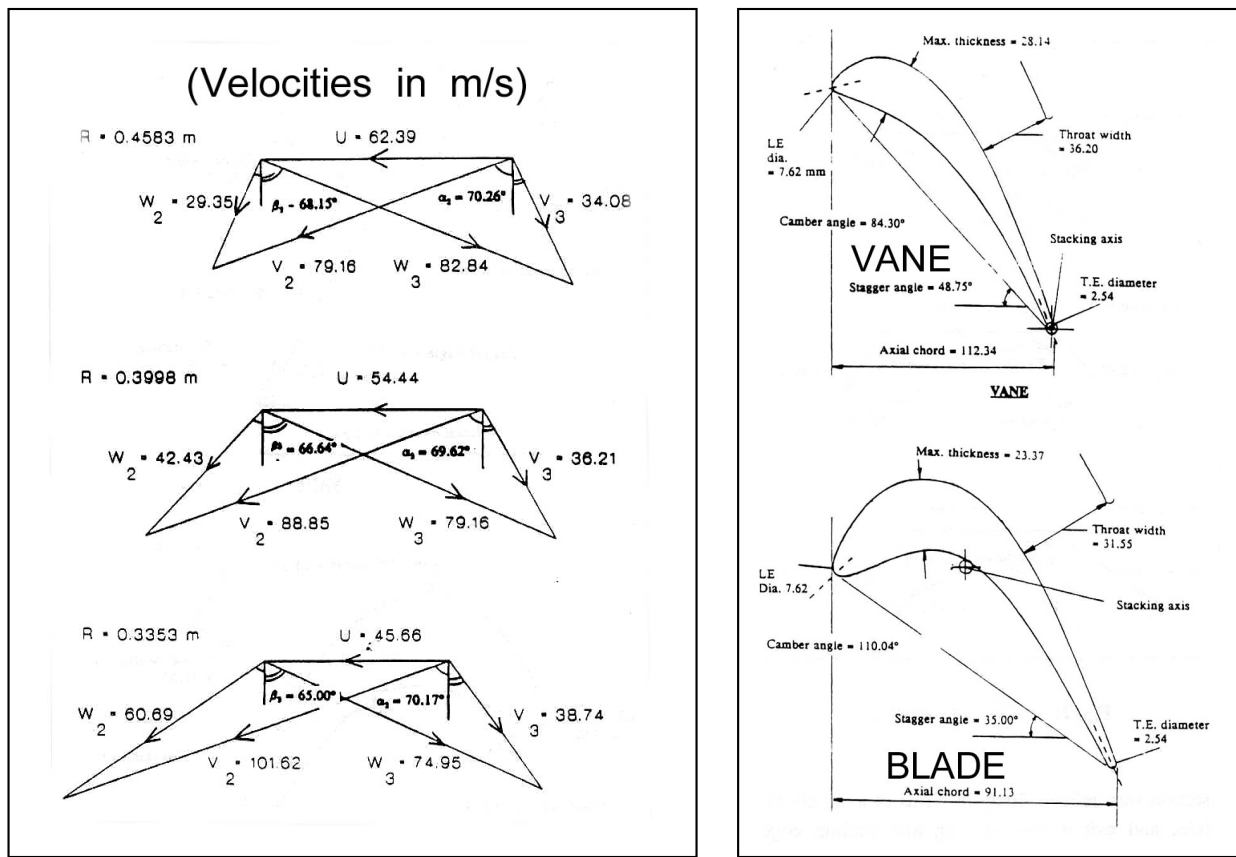


Figure 2. Blade velocity triangles at the hub, mid-radius and tip in AFTRF, vane and blade geometry at mid-span , © AIAA

A two-dimensional through-flow analysis solved the circumferentially-averaged equations of motion in the meridional plane, using a streamline curvature technique Smith,[3]. This accounted for blade forces, blade blockage, aerodynamic losses, and real gas effects. Losses were accounted for in the current design by carrying through the area average stage efficiency obtained from the loss model in the optimized one-dimensional mean line study, and inputting it to the through-flow analysis as a radial distribution of constant efficiency. The real, three-dimensional, viscous effects of secondary flows, tip leakage, etc., and their subsequent mixing with what may be termed the primary flow, has not been considered in terms of local features. The best means to accomplish this in practice would be

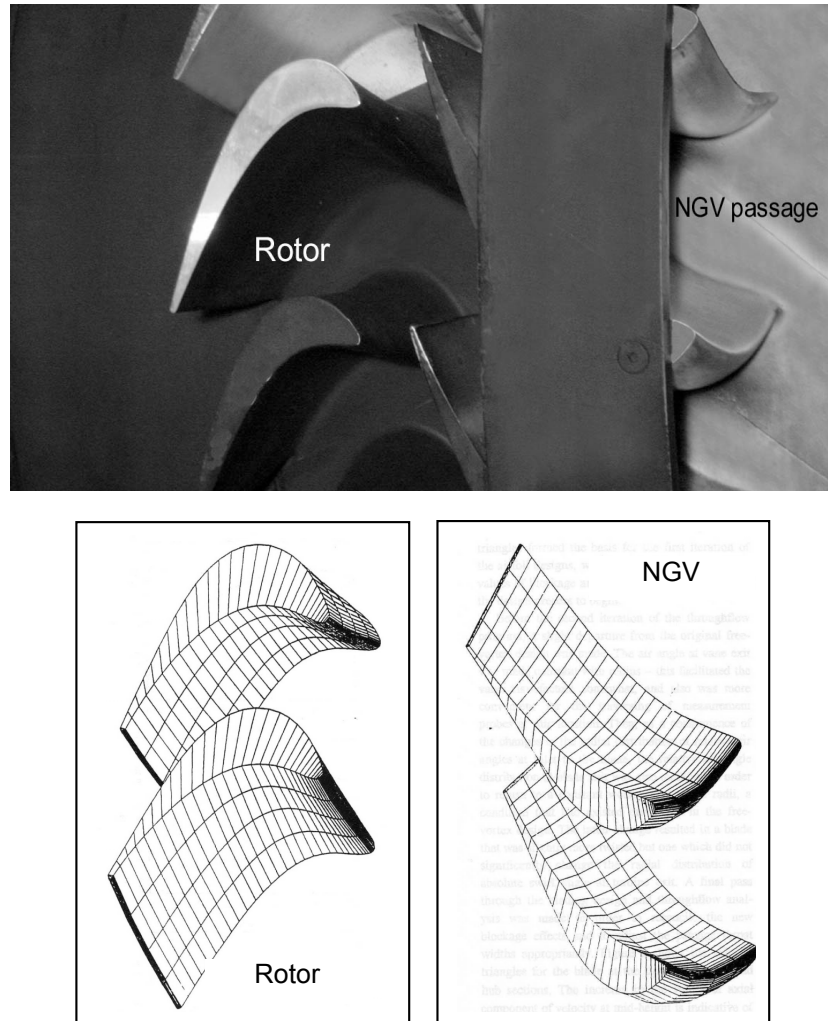


Figure 3. AFTRF stage and the wire-mesh models of the vanes and blades , © AIAA

to incorporate the results of detailed measurements from the current turbine rig in the input data for a future improved design - the key to successful development in the aero-engine industry. The input file for the circumferentially-averaged analysis was generated initially using the free-vortex radial distributions from the optimized mean-line study discussed in the previous section. Radial distributions of all geometric and aerodynamic parameters were defined at 11 streamline locations.

At the beginning of the through-flow analysis the airfoil sections had not been designed, so proper account could not be taken of blade blockage and losses. The first pass through the program produced estimates of velocity triangles which were consistent with the required turbine work and efficiencies defined earlier in the 1-D model. These velocity triangles formed the basis for the first iteration of the airfoil designs, which resulted in more realistic values of blockage and enabled the second cycle of the design process to begin.

Before the second iteration of the through-flow program, a slight departure from the original free vortex design was made. The air angle at vane exit was made constant with radius - this facilitated the vane manufacture somewhat, and also was more convenient for the traversing of measurement probes at this location. Then, as a consequence of the changes to the radial distribution of relative air angles at inlet to the blade, the relative air angle distribution at blade exit was also modified in order to return to a constant work output at all radii, a condition that had existed previously in the free-vortex

design. The latter change resulted in a blade that was slightly more twisted but one which did not significantly change the radial distribution of absolute swirl angle at turbine exit. A final pass through the blading design and through-flow analysis was made in order to reconcile the new blockage effects and to adjust the passage throat widths appropriately. Figure 2 shows the velocity triangles for the blade at the tip, mid-height, and hub sections. The increase in the values of axial component of velocity at mid-height is indicative of a corresponding reduction in static density of the working fluid as it passes through the parallel annulus.

Table 1
Design and Target Performance Parameters

	DESIGN	TARGET
Total temperature at inlet ($^{\circ}$ K); T_{∞}	289	289
Total pressure at inlet (kpa); P_{∞}	101.36	101.36
Mass flow rate (kg/s); W	11.05	
Specific work output (kJ/kg); $\Delta h_o/W$	5.49	
Flow function; $W\sqrt{T}/P$ ($\text{kg}\sqrt{\text{K}} \text{ m}^3/\text{kN} \cdot \text{S}$)	1.85	1.85
Energy function ($\text{kJ/kg} \cdot \text{K}$); $\Delta h_o/T$	0.019	0.019
Speed function ($\text{rpm}/\sqrt{\text{K}}$); N/\sqrt{T}	77.69	
Rotational speed; N 1300 rpm	1250 rpm	
Total pressure ratio; $P_{\text{out}}/P_{\infty}$	1.0778	1.0778
Total temperature ratio	0.9810	
$T_{\text{out}}/T_{\infty}$		
Pressure drop (mmHg); $P_{\infty} - P_{\text{out}}$	56.04	
Hub reaction; R	0.181	0.20-0.35
Pitchline reaction; R	0.3820	0.40-0.5
Pitchline loading coefficient; ψ	3.76	3.4
Hub loading coefficient; ψ	5.27	
Stator Zweifel coefficient	0.7247	0.70
Rotor Zweifel coefficient	0.9759	0.90
Power (kw)	60.6	
Stator efficiency; η_s	0.9421	
Rotor efficiency; η_r	0.8815	
Total-to-total; η_{TT}	0.8930	0.90
Isentropic efficiency		

Table 2
The Design Features of AFTRF

Hub Tip Ratio	0.7269
Tip Radius	0.4582 m
Blade Height	0.1229 m
Tip Rel. Mach Number	0.240 (max)
Rotor Blade (tip) number	29
chord	0.1287 m
spacing	0.1028 m
turning angle	95.42° (tip), 125.69° (hub)
maximum thickness	22 mm
tip clearance	1.27 mm (actual 0.97 mm av., 1.04 mm max, 0.77 mm min)
Nozzle Guide Vane (tip) number	23
chord	0.1768 m
spacing	0.1308 m
turning angle	70 deg.
maximum thickness	38.81 mm
Auxiliary Fan pressure rise	74.72 mm Hg
mass flow	10.39 m ³ per sec. (22,000.0 cfm)
power	149.1 kw
Vane Reynolds Number based on inlet vel.	(3 ~ 4) x 10 ⁵
based on exit vel.	(9 ~ 10) x 10 ⁵
Blade Reynolds Number based on inlet rel.vel.	(2.5 ~ 4.5) x 10 ⁵
based on exit rel.vel.	(5 ~ 7) x 10 ⁵

The nozzle and the blade were designed at five streamline sections corresponding roughly to 10,20, 50, 70 and 90% of the annulus height as shown in Figure 3. The design technique consisted of the following: (a) definition of the geometry of each airfoil section, (b) stacking the blade and checking that all geometric parameters varied smoothly over the airfoil height, (c) running a blade-to-blade aerodynamic solution for each streamline surface, (d) making adjustments to geometry and aerodynamic blockage where necessary and repeating the cycle until a satisfactory airfoil design was achieved.

By running blade-to-blade solutions in conjunction with the circumferentially-averaged through-flow analysis in the meridional plane, a quasi three-dimensional design was obtained. Each section was defined firstly in terms of axial chord, inlet and exit angles, leading and trailing edge diameters, passage throat width, stagger angle, and uncovered turning on the back surface. The final

airfoil shape was then specified in terms of surface curvature and an elliptical leading edge profile. Following the first aerodynamic analysis of the airfoil section, an adjustment was made to the inlet angle to allow for induced incidence effects. The isometric views of the vane and blade are shown in Figures 3. For convenience the vane sections were stacked on a radial line passing through their trailing edges, and for structural reasons, the blade sections were stacked on a radial line through their centers of gravity. The overall performance parameters of the turbine stage are given in Table 1 and the final design features of the blading are presented in Table 2.

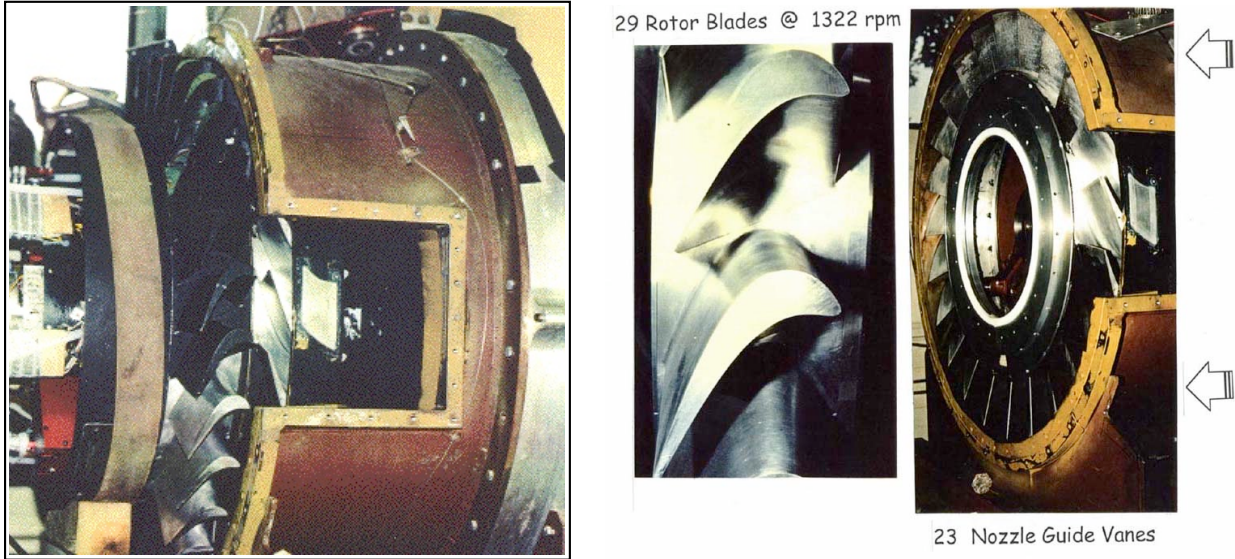


Figure 4. AFTRF stage (outer casing removed)

There is an obvious dichotomy in the design of a high pressure turbine (HPT) for a low-speed, low-pressure facility. Yet there is also a need and a desire to investigate certain HPT flow phenomena economically by means of such a vehicle. One of the objectives of the present exercise was to ascertain which aspects of an HPT design it was possible to duplicate.

Clearly the direct simulation of many compressibility effects is not possible. Mach numbers in excess of unity and associated phenomena such as shocks and expansion waves cannot exist without the availability of a high overall pressure ratio to sustain them. It is entirely possible however to apply the rules of aerodynamic similarity to relate the current low speed blading to those they would model in the real engine situation. The success of such a modeling procedure has been clearly demonstrated by Wisler,[4]. The effects of differences in Mach number on dimensionless body forces or pressure coefficient between prototype and the model may be accounted for by increases in angle of attack, camber, and airfoil thickness in the model and this is done in an iterative manner using a reliable prediction technique. Additionally, in model testing, care must be taken to ensure that scaled surface roughnesses are used and that the turbulence intensities and the Reynolds numbers are duplicated.

Many parameters associated with HPT performance may be represented exactly, since they are usually expressed non-dimensionally. Examples of these are stage loading coefficient $2\Delta h_o/U_m^2$, flow coefficient V_x/U_m , flow function $\sqrt{\theta}/\delta$, stage reaction, and Zweifel coefficient. Also, in an absolute sense, high blade turning angles and Reynolds numbers may be replicated, while many geometric features such as blading aspect ratio and solidity pose no problems. The measure of success in this regard may be gained from the data presented in Tables 1 and 2. The final stage design is presented in Figure 4 without AFTRF outer casing. In the design of the airfoil shapes, the inability to generate high

exit-to-inlet velocity ratios and abrupt decelerations via shock waves in the blading passages was of some concern. Some early attempts were made to reproduce HPT blade surface velocity profiles in a non-dimensional sense (although without the effects of shock waves), but this led to airfoil shapes which were incorrect geometrically and aerodynamically, and would have been totally inappropriate for such research work as the study of boundary layer development, etc. It is felt that a good compromise has been reached in the ensuing design - one that will optimize the use and effectiveness of the turbine rig for many years to come.

AIRFOIL SURFACE VELOCITY DISTRIBUTIONS

With reasonable care in the leading edge design, diffusion just aft of the leading edge on the pressure surface was avoided. By suitable choice of suction surface curvature and the degree of uncovered

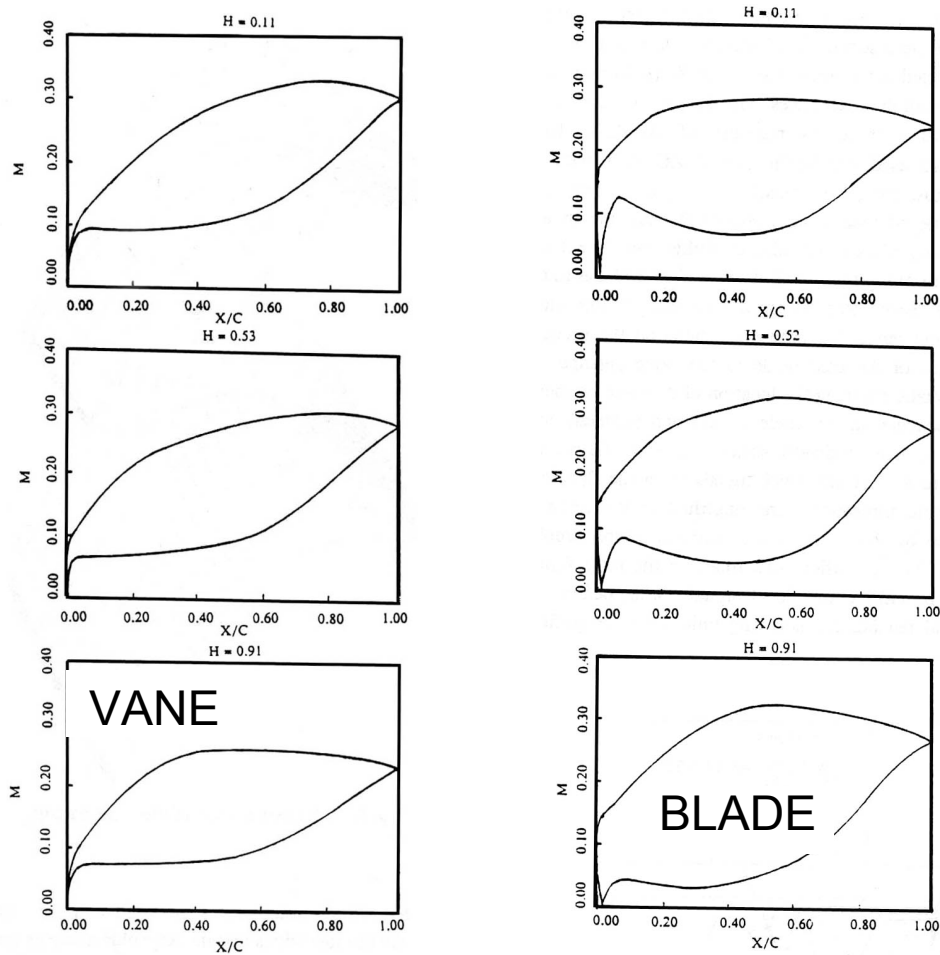


Figure 5. AFTRF velocity distributions (predicted Mach numbers) at the hub, mid-span and tip sections . ©AIAA

turning, the locations and magnitudes of the peak velocities were controlled so as to produce only very modest values of suction side diffusion on all design sections. These characteristics are shown in Figures 5 for vane and blade.

Although the overall stage pressure ratio was small, a relatively high value of stage loading coefficient, $2\Delta h_0/U_m^2$, had been selected, which was typical of high pressure turbines existing in present day engines. In order to produce the power needed, high turning was required in the blade passage, particularly near the hub, where it is 126° . This high turning tended to produce high values of peak velocity on the suction surface with subsequently large, undesirable amounts of diffusion as the air returned to the relatively low value of velocity at the exit. It was attempted to limit the back surface diffusion to 20% of the exit velocity value. The success of this can be judged from Figure 5, where predictions of the blade surface Mach number distributions are plotted.

The other significant concern in the design of the airfoils with regard to performance was in limiting the over-speeding on the suction surface just aft of the leading edge. On any turbine blade the flow is subject to high acceleration around the leading edge region on both the suction and pressure surfaces. In both cases there may be a subsequent undesirable localized diffusion where the surface curvature is reduced as the leading edge blends with the flanks of the airfoil. A local diffusion, however small, is of more concern on the suction side, where it may constitute a very significant disturbance to the (laminar) boundary layer, possibly resulting in airflow separation. In the present blading design it was possible to trade off suction-side diffusion for pressure-side diffusion by precise tailoring of the leading edge contour, and adjustment to its inclination (incidence). The choice of leading edge inclination was also influenced by the "induced incidence" produced as a result of the circulation existing around any particular airfoil section. The vane was designed with greater cross-sectional areas at hub and tip than at the mid-span. This resulted in greater circulations at the ends of the airfoil than in the mid-height and a corresponding distribution of induced incidence. The leading edge of the vane is therefore bowed as can be seen in Figure 3. A radial variation of leading edge inclination was also used on the rotor blade both to balance out the effects of over-speeding around the suction and pressure sides of the leading edge and to eliminate the effects of induced incidence caused by flow turning (lift on the blade) and by thickening of the airfoil in the hub region. Generally only a very slight tendency to over-speed was tolerated on the suction surface, which is hardly discernible in Figure 5, as it was felt that any consequent minor increase in over-speeding and local diffusion on the pressure surface would not affect blade performance significantly. The general increase in pressure surface diffusion on the rotor blade as the hub section is approached, which may be seen in Figure 5, is due largely to the simple structural requirement for more cross-sectional area in this region of the blade.

DETAILS OF FACILITY INSTRUMENTATION

Blade and Vane Surface Instrumentation: The Axial Flow Turbine Research facility is equipped with a large number of static pressure holes (nearly 500) at carefully selected locations inside one vane passage, inside one rotor passage, nozzle end wall and rotor endwall regions. Static pressure measurements in the rotating frame are taken by a 32 channel electronic pressure scanner located in the rotor frame. The signal output, after multiplexing in the rotor frame, is passed through a slip ring unit for processing in a computer controlled data acquisition system. The specific system collects data mainly for steady performance measurements at a total sampling rate of 20 KHz.

One of the most attractive and convenient methods for measuring the wall shear stress is through the use of a hot film shear stress gauge (McCroskey and Durbin,[5]). The technique is based on the principle of relating the convective heat transfer (from the gauge to the fluid) to the local shear stress. This is the technique adopted for use in the Axial Flow Turbine Research Facility. The thin film thickness of 50 microns is thinner than the viscous sublayer that will be encountered in the internal flow passages of the turbine facility. McCroskey and Durbin's [5] approach is used for the measurement of shear stress direction. They employ two similar thin films arranged in a V shape.

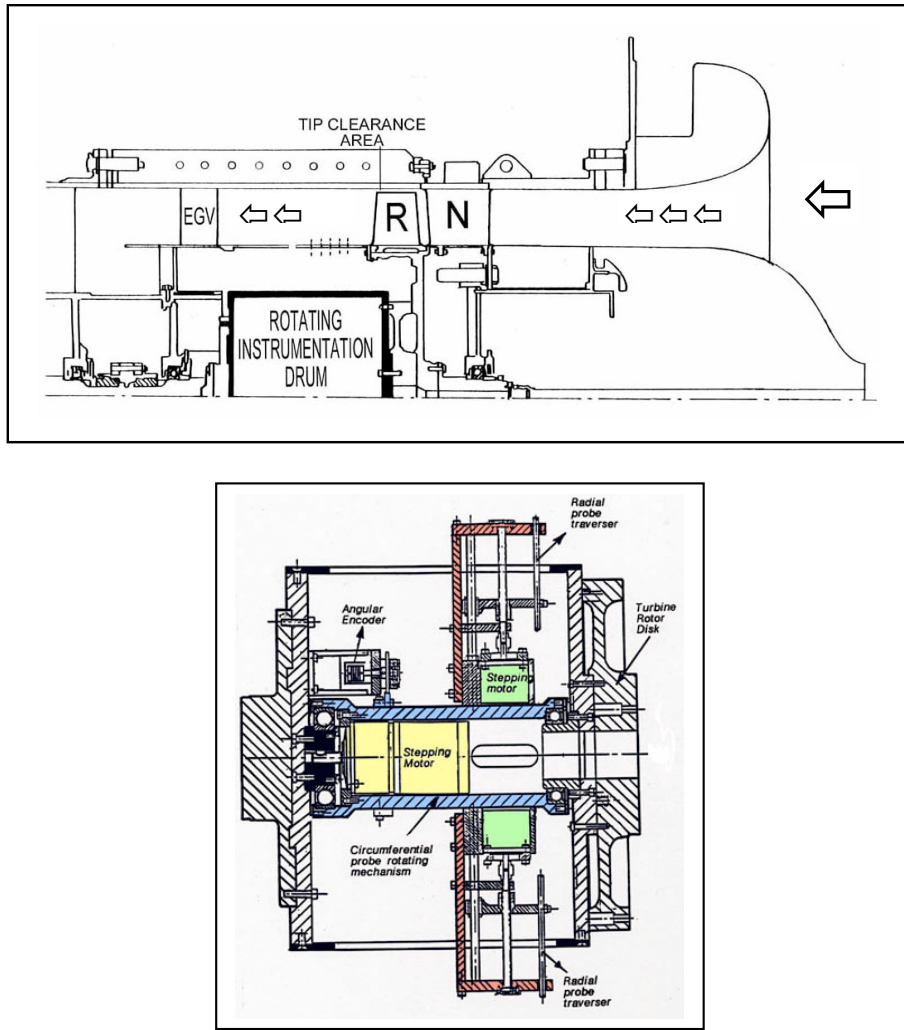


Figure 6. AFTRF rotating instrumentation drum and probe traversing system
(radial and circumferential probe motion with respect to the rotor)

A shear stress gauge is constructed to provide both the direction and magnitude of the shear stress vector. Knowledge of the direction of the wall shear stress is extremely critical in turbomachinery flows where three dimensional viscous flows are encountered. This V-configuration type shear stress sensor may also be used to detect the onset of separation point in a flow as indicated by " $\tau_w = 0$ ". The specific shear stress sensors used in the turbine rig are the deposited thin film (V array) "glue on dual probes" manufactured by Dantec Inc. A total of 23 dual element sensors are mounted around the rotor blade at mid span, with close spacing near the leading edge of the blade. In addition, five sensors are located on the hub (endwall) of the rotor blade passage. The sensors are located in one passage, on both the pressure and the suction surfaces. The signals are brought into the rotating drum shown in Figure 6. Unsteady shear stresses, which are important quantities in the study of vane-blade interaction, are recorded by a high speed data acquisition system.

A complete understanding of unsteady rotor stator interaction requires a measurement system capable of measuring the instantaneous unsteady dynamic pressures. The implementation of the dynamic pressure transducers in the turbine rig was driven by space limitations. The pressure transducers are inserted into chambers, which in turn are connected to the turbine airfoil surfaces through 0.5 - 0.8 mm diameter holes. The design objective is to achieve a frequency response of 40

KHz. The sensors used are Kulite model XCS-093 with a pressure range of maximum 5 psia. They are capable of measuring pressure fluctuations to an accuracy of 0.01 psia. Sixteen Kulite transducers are located along the chord at the mid-span of the rotor blade. Seven transducers are on the pressure side and the remaining nine are located on the suction surface of the next blade in the same passage. The low level signals from the dynamic pressure transducers are amplified in the rotating frame by using miniature instrumentation amplifiers. The amplifiers will rotate in the rotor frame of reference and provide a high level signal output before the signal reaches the slip ring unit. These amplifiers are located inside the rotating instrumentation drum shown in Figure 6.

Provision is also made for the same amplifiers to be interfaced with other low level signals such as shear stress gauges, heat flux sensors, and hot wire sensors. Data logging for fast response instruments such as Kulites and thin films are performed on a high speed data acquisition system with a sampling capacity of at least 100 KHz per channel.

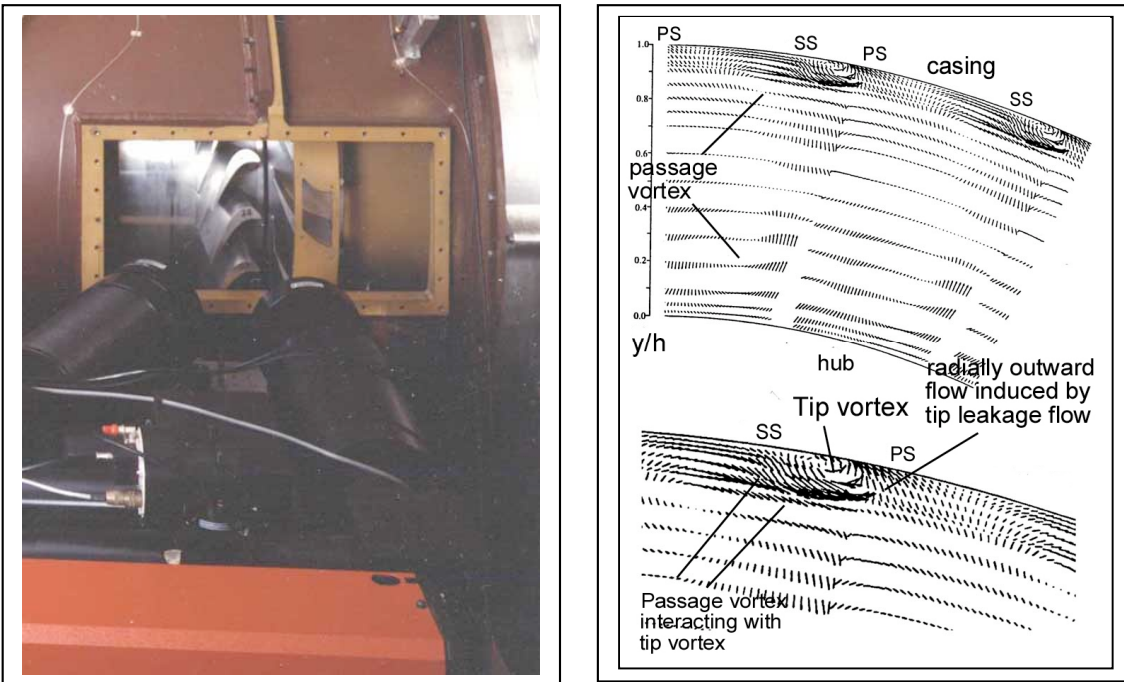


Figure 7, AFTRF 3D Laser Doppler Anemometer (LDA) near the optical window and rotor exit LDA measurements showing the tip vortices and passage vortex system (phase locked measurements of Ristic et al. [8])

Rotating Frame Measurements: Provision has been made for hotwire and conventional probe measurements in both the rotating and the stationary system. Both two sensor and three sensor hot wire probes are used in a stationary frame of reference to measure the boundary layers on stationary walls (on both the casing and hub walls) and the nozzle vane surface. The mechanism used for traversing the rotating hotwire probe and the five-hole probe consists of both the circumferential and the radial traversing units. The rotating probe traverse device is shown schematically in Figure 6. The hotwire probe location can be incrementally changed by using 0.019 degree steps, in a circumferential direction. This motion is also checked and corrected for possible errors by an angular encoder device. The planetary gearbox providing this precision motion is driven by a stepping motor having 25000 steps per revolution. Both the radial and circumferential traversing units are simultaneously controlled

by a computer based system. The interface between the computer and the rotating drum is provided through a 150 ring slip ring device. The two and three sensor hot wire technique for the measurement of stationary flows (nozzle wakes, boundary layer) as well as rotor shear layer is described by Lakshminarayana [6].

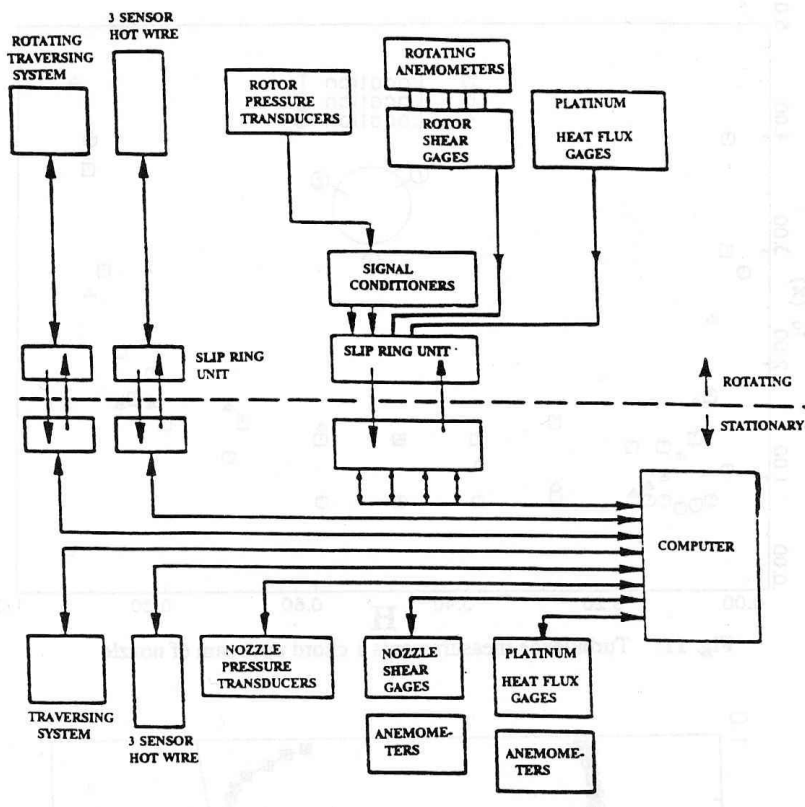


Figure 8. Rotating and stationary measurement system interface to the computer data acquisition system

Through the proper use of LDA and hot wire sensors, the entire steady and unsteady flow field, including the wall layers, can be measured in the turbine stage. The LDA system available in the Turbomachinery Laboratory is a three channel fringe type laser Doppler anemometer (LDA) with on-axis back scatter light collection. The system operates with a 7 W Coherent Argon-ion laser. The entire system comprising the laser, the transmitting and receiving optics is mounted on an optical bench. The precision bench can be moved along and perpendicular to the optical axis and can also be tilted in the vertical plane. The assembly is fitted on a hydraulic lift table capable of moving in the vertical direction. The three degrees of freedom with a possibility to tilt the table helps to position the bisector of the beam in the radial direction. The signal from the photo-multiplier tube is fed into three counter type signal processors (TSI Model 1998). The counter measures the period for eight cycles of the Doppler burst. The counter also validates and digitizes the signal. Three input/output units, counter timer and an electronic coincidence filter interface with three counters to a computer. A typical application of the previous two component LDA system at Penn State is given by Murthy and Lakshminarayana [7]. An electronic encoder system provides the angular position of the measurement with respect to a given rotor passage. The computer records simultaneously the tangential velocity component, the axial velocity component, and the angular position. The flow upstream and

downstream of the rotor and inside the rotor are acquired using the LDA system. A more recent application of the LDA principle by Ristic et al. [8] in the turbine environment is shown in Figure 7. The particular results shown in Figure 7 are from three component LDA measurements including the radial component of the velocity vector. Acquisition of the radial component in addition to axial and tangential components is extremely important in resolving the 3D structure of passage vortices and tip vortex in the passages.

Data Transmission, Acquisition and Processing: The Kulite, skin friction, heat transfer, hot wire and static pressure data from the rotor will be transmitted through the rotating drum to a 150 channel slip ring unit. The rotating drum (Figure 6 and 7) consists of two probe traversing mechanisms for both the radial and the circumferential traverse, 4 constant temperature anemometers, a 32 channel electronic pressure scanner/transducer unit and a 30 channel data acquisition system for voltage inputs. The data acquisition system interface to the computer is shown in Figure 8. A medium speed data acquisition system with 96 channels of pressure transducers having a 20,000 samples per second capacity is used. The PSI model 780-B pressure measurement system is a fully integrated test instrument which offers a transducer per port for multipressure measurement applications. The system is interfaced to a desktop computer through an IEEE-488 with input-output rates up to 30,000 bytes per second. For high speed data acquisition, a 16 channel, 12 bit transient recorder with a 1 Megabyte solid state memory is used. The acquisition system is controlled by a parallel bus controller interfaced to a desktop computer. With the current configuration, the system is able to store 4,000,000 measurements for a typical duration of one second either in its own memory or in the computer storage medium. The main use of this system is in the area of wall shear stress, Kulite dynamic pressure and unsteady heat transfer measurements. The same system can be used for acquiring hotwire data and resolving the deterministic and random unsteadiness in the rotor flow.

Performance Measurements at Near Design Condition: In order to check for the flow axisymmetry upstream of the nozzle and to determine the turbulence intensity upstream of the nozzle, a single sensor hot wire probe and a sub-miniature five-hole probe are used to measure the radial distribution of axial turbulence intensity and mean velocities at three tangential locations (120 degrees apart) at the inlet. The axial turbulence intensity, shown in Figure 9, is nearly constant at around 0.75 to 1.5 percent, except near the hub and casing. The axial velocity is found to be nearly identical at these locations. The stagnation pressure is nearly uniform, with the exception of locations inside the wall boundary layer. The static pressure is also uniform radially. The measured axial, tangential and radial velocity profiles are shown in Figure 10. The free-stream velocity is 27.2 m/s with a Reynolds number of 3.30×10^5 based on a basic nozzle vane chord at mid-span. The wall boundary layers are turbulent, with a thickness of approximately 5% blade span at the hub and 10% blade span at the tip. These figures also show that the radial and tangential velocities are almost negligible upstream of the nozzle.

Overall Performance: The performance measurements are carried out at four different mass flows at the corrected design speed of (1300 RPM). An in-house manufactured sub-miniature five hole probe with a maximum diameter of 1.67 mm is used. The five-hole probe data included a large number of radial stations, with close intervals inside the hub and annulus wall boundary layers. Hence the mass flow calculated includes the blockage due to the annulus and the hub wall boundary layers. The pressure drop coefficient (loading coefficient) is mass averaged based on the local axial velocity at exit (location 3) given by :

$$(\bar{\psi}) = \frac{\int_{hub}^{tip} \psi V_{x3} 2\pi r dr}{\int_{hub}^{tip} V_{x3} 2\pi r dr} \quad (1)$$

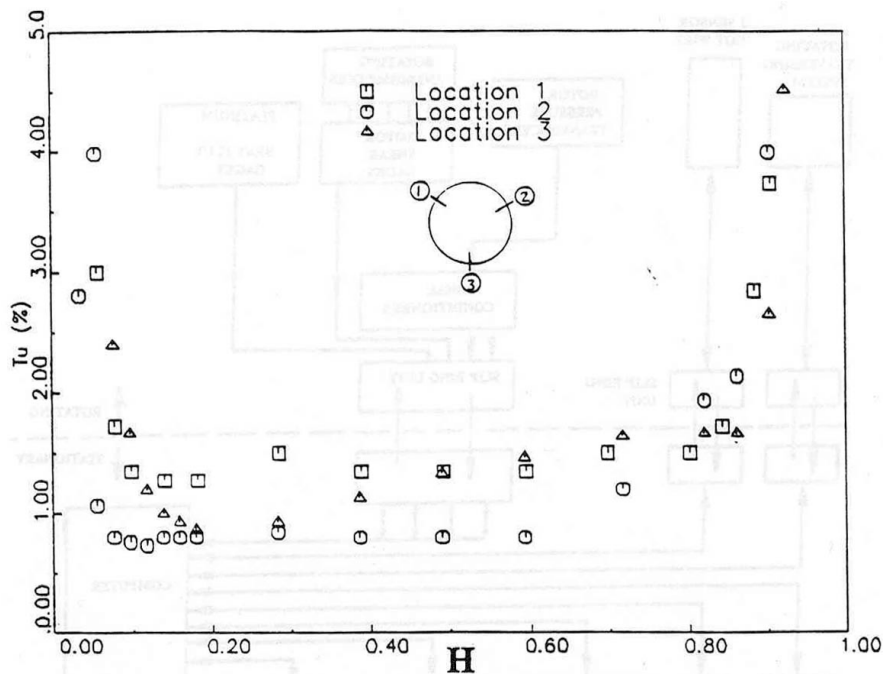


Figure 9. Turbulence intensity measurements one chord upstream of the nozzle guide vanes, ©AIAA

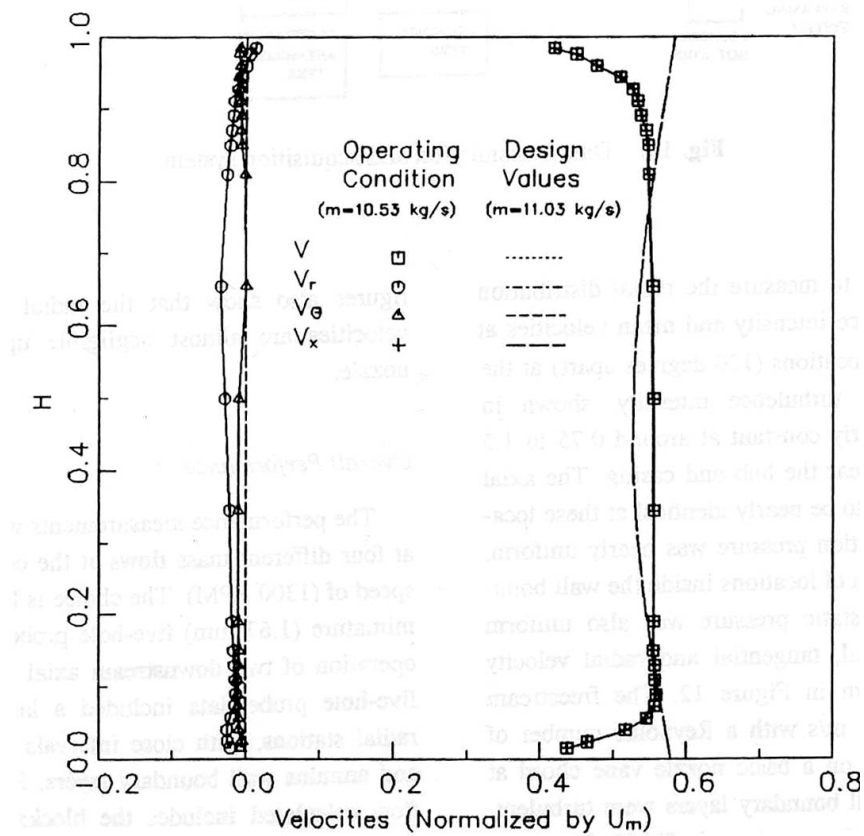


Figure 10. Radial distribution of measured velocity profiles upstream of the nozzle guide vanes, ©AIAA

The mass averaged pressure drop coefficient is shown plotted against corrected mass flow in Figure 11. As expected, the loading coefficient varies linearly with an increase in the mass flow and the measured loading coefficients near the design mass are very close to the design value. The facility is operated at $m = 10.53 \text{ kg/s}$ during the research phase of the program. The mass averaged pressure drop coefficient is closely matched at the design and operating conditions.

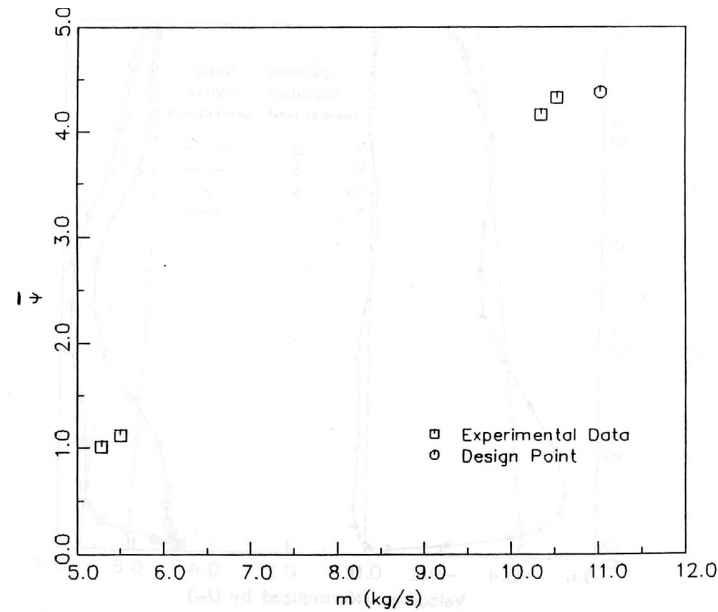


Figure 11. Loading coefficient versus mass flow rate in AFTRF, ©AIAA

Rotor Exit Measurements: The radial distribution of total and static pressures, total, axial, radial and tangential velocities, and rotor exit flow angle at design conditions were measured two chords downstream of the rotor blade row using a five-hole probe. Figures 12 through 14 show the experimental data measured close to the design point ($m = 10.53 \text{ kg/s}$). These results are compared with the design distribution at $m = 11.03 \text{ kg/s}$, which is close to the operating condition.

The radial distribution of stagnation pressure drop coefficient (loading coefficient ψ) and the static pressure drop coefficient (ψ_s) are shown compared with values at the design point in Figure 12. The cumulative effect of nozzle and rotor secondary flow near the hub wall results in higher loading coefficient in this region. The leakage flow and the resulting under-turning is responsible for lower loading coefficient in the tip region ($H > 0.95$). The under-turning is prevalent in 5% of the span from the tip. The secondary flow, which overturns the fluid, has a major effect in increasing the pressure drop, reaching a maximum value at $H \approx 0.90$. The minimum pressure drop occurs near the mid-span, while the maximum pressure drop occurs near the hub and the endwall region. Hence, this flow is dominated by the hub and the annulus wall secondary flows and the tip leakage flow. The presence of loss core in the hub region, which moves radially outward, results in lower loading coefficient (due to higher losses) away from the hub wall. This is evident from the loading coefficient distribution away from the hub and the annulus walls. The profile boundary layer losses are also substantial in these regions.

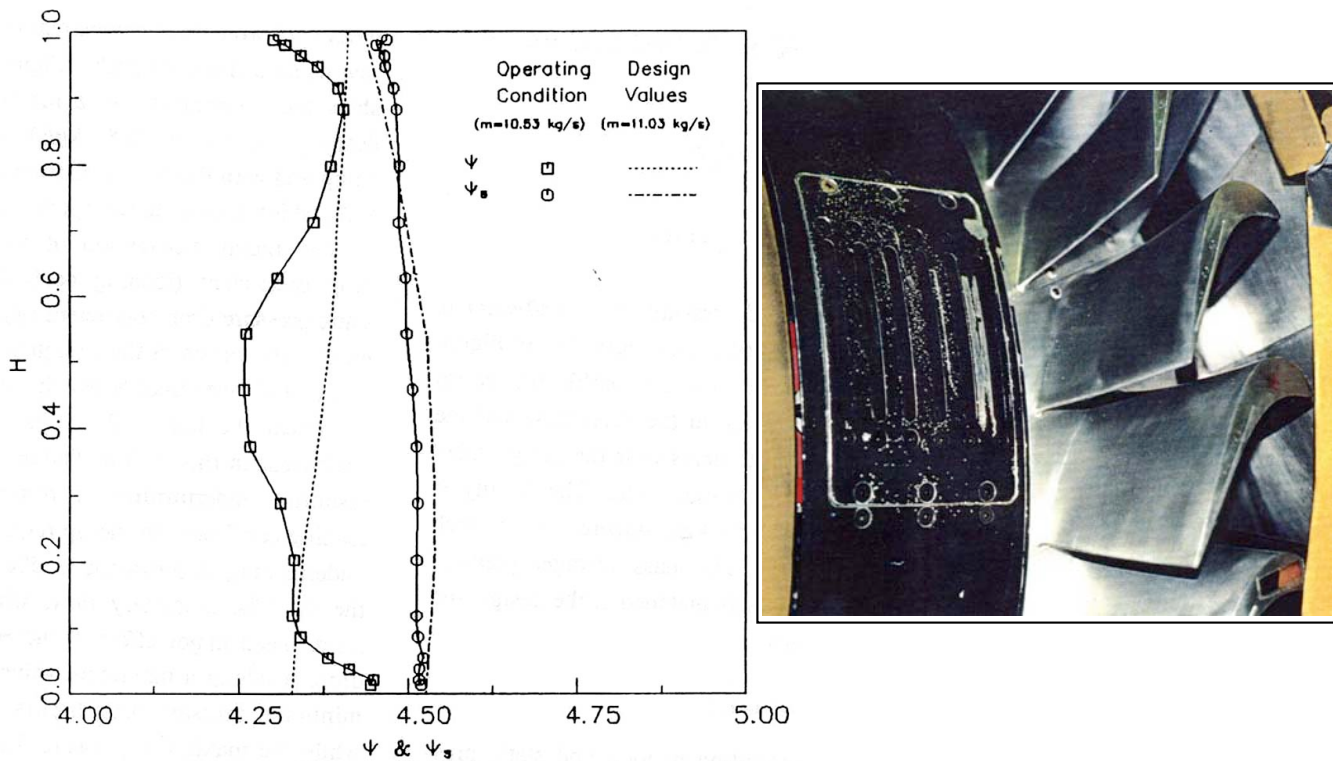


Figure 12. Radial distribution of measured stagnation and static pressure drop coefficient in AFTRF (rotor exit/far downstream), © AIAA

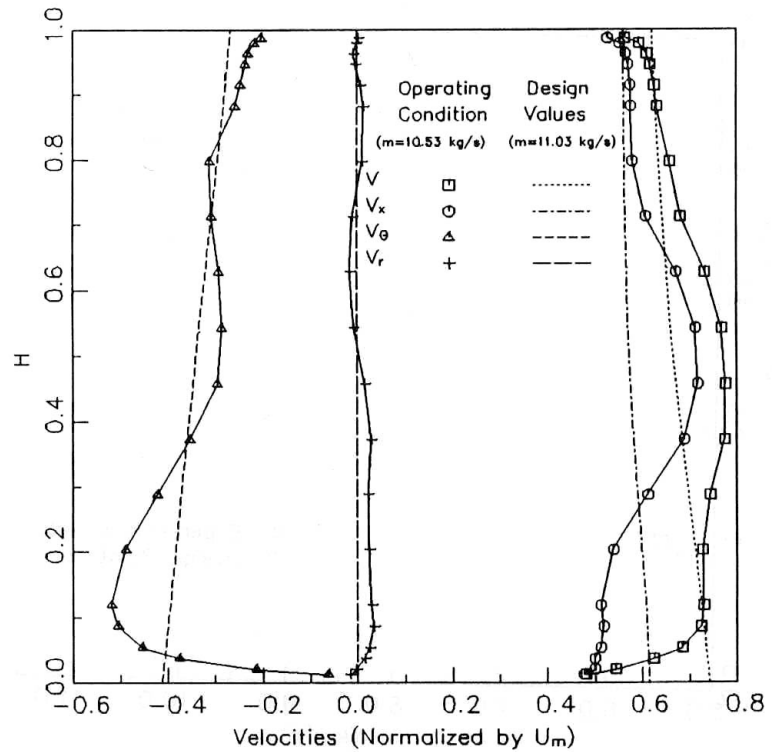


Figure 13. Radial distribution of axial, radial and tangential velocity (absolute) components in AFTRF (rotor exit/far downstream), © AIAA

The radial variation of axial, tangential and radial velocities are plotted in Figure 13. The radial velocities are negligibly small at this far downstream location. The presence of a loss core results in lower axial velocity in the hub region, and flow acceleration in other radial locations (e.g., $H = 0.3$ to 0.7). The presence of the secondary flow and wall boundary layer results in low velocities in the hub and tip regions. These loss core regions tend to increase flow blockage giving rise to acceleration of the flow near the mid-span region.

Similar distributions have been reported by Joslyn and Dring [9] and Boletis and Sieverding [10]. The tangential velocity distribution shows a similar trend. Near the hub wall (from $H = 0$ to 0.05) the effect of the wall boundary layer is evident. Higher tangential velocities are observed in the region $0.04 < H < 0.4$. The tangential velocities are close to design at most other locations, with the exception of the tip regions. The effect of leakage flows are clearly seen in the region $H > 0.95$, where the tangential velocities are lower.

These distributions are consistent with angle distributions (absolute flow), shown in Figure 14. The pitch angles are very small. The overturning of the flow near the hub wall and under-turning in regions away from the hub wall is evident from Figures 13 and 14. The overturning region is confined to $0.04 < H < 0.3$ in the hub region. Substantial deviation from the design distribution of yaw angle is evident from Figure 14. The yaw angles show substantial overturning in regions $0.04 < H < 0.3$, under-turning in the middle third of the blade and under-turning in regions $H > 0.8$.

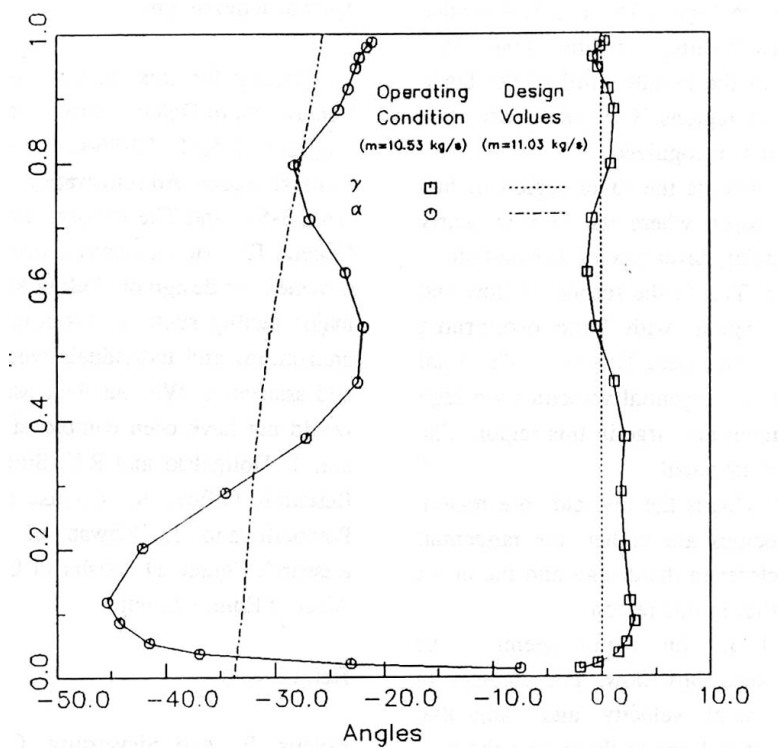


Figure 14, Radial distribution of pitch (γ) angle and yaw angle (α) (rotor exit/far downstream) . © AIAA

Hence, five distinct regions can be recognized:

- 1) $0 < H < 0.04$: This is the inner region of hub wall boundary layer, where the flow is nearly axial, with boundary layer type of distribution.
- 2) $0.04 < H < 0.3$: This is the secondary flow and the loss core region, with large overturning (reaching peak value near $H = 0.1$). The axial velocities are low, tangential velocities are high and the yaw angles are large in this region. The radial velocities are small.
- 3) $0.3 > H < 0.7$: This is the inviscid core region. The axial velocities are higher, the tangential velocities are closer to the design and the outlet angles are smaller in this region.
- 4) $0.7 < H < 0.95$: This region seems to be influenced by secondary flow. The changes in outlet angle, axial velocity and tangential velocities are not as large as those near the hub. But the fact that the flow is overturned with respect to the design indicates the presence of secondary flow in this region.
- 5) $H > 0.95$: This region is dominated by tip leakage effect, with appreciable under-turning, low tangential and axial velocities.

These exit flow distributions are consistent with the measurements by Joslyn and Dring [9] and Boletis and Sieverding [10] measured at the exit of a turbine stage.

Intra-stage coolant injection system : A special coolant (or leakage) air delivery system exists between the nozzle guide vanes and the rotating disk assembly of AFTRF. Figure 15 shows the three individual coolant injection chambers built into a precision machined flat concentric plenum chamber. The chamber is attached to the NGV assembly in the stationary frame and positioned between the flat surface of the rotating disk and NGV. The first chamber is termed as disk impingement cooling system that is capable of delivering discrete coolant jets (normally) impinging on the rotating disk. The disk cavity is sealed by using a circular Teflon seal at the inner radius (the white ring in Figure 15).

An injection scheme sending coolant (or leakage) air in the radially outward direction forms the middle chamber of the concentric plenum chamber presented in Figure 15. Radially outward injection is sent into the disk cavity area. The disk impingement plenum and the radial injection plenum supply coolant air into 23 discrete holes of 6 mm diameter. There is one hole for each nozzle passage (in each chamber) in AFTRF.

The root injection plenum system sends coolant air directly into the mainstream at 45 degrees measured from the hub surface. The root injection jets are precisely aligned with the nozzle vane trailing edge direction so that the injection air has a chance to fill in the wakes of the nozzle guide vanes. The beneficial aerodynamic effects of root injection from nozzle guide vane trailing edges are explained in McLean and Camci [11] and [12]. The same publications also discuss the influence of using disk impingement jets and radial injection holes delivering coolant air into disk cavity space.

Stationary-to-rotating frame air transfer system: The aerodynamic and heat transfer studies requiring cooling air in the rotating frame of reference require an air transfer system that is capable of bringing coolant air into the turbine blade roots without significant leakage and flow disturbance. Figure 16 shows the details of such a system installed in the middle bearing location of AFTRF shown in Figure 1. The two stationary precision seals working against plasma coated surfaces in the rotating side of the air transfer system provide minimized “coolant leak”. The integration of this air transfer system into the middle bearing area of AFTRF is explained in Figure 16. Once the cooling air is transferred to the rotating instrumentation drum, a precision orifice based mass flow rate measurement system meters the coolant flow rate into the cooled blades (or other parts of the rotor). A pair of rotating pressure transducers measures the mass flow rate of coolant air. The current system is optimized for blade tip injection studies. Five individual blades have plenum chambers installed at blade roots for various tip injection studies in AFTRF. A detailed description of this system can be found in Dey&Camci [13] and Rao&Camci [14], [15].

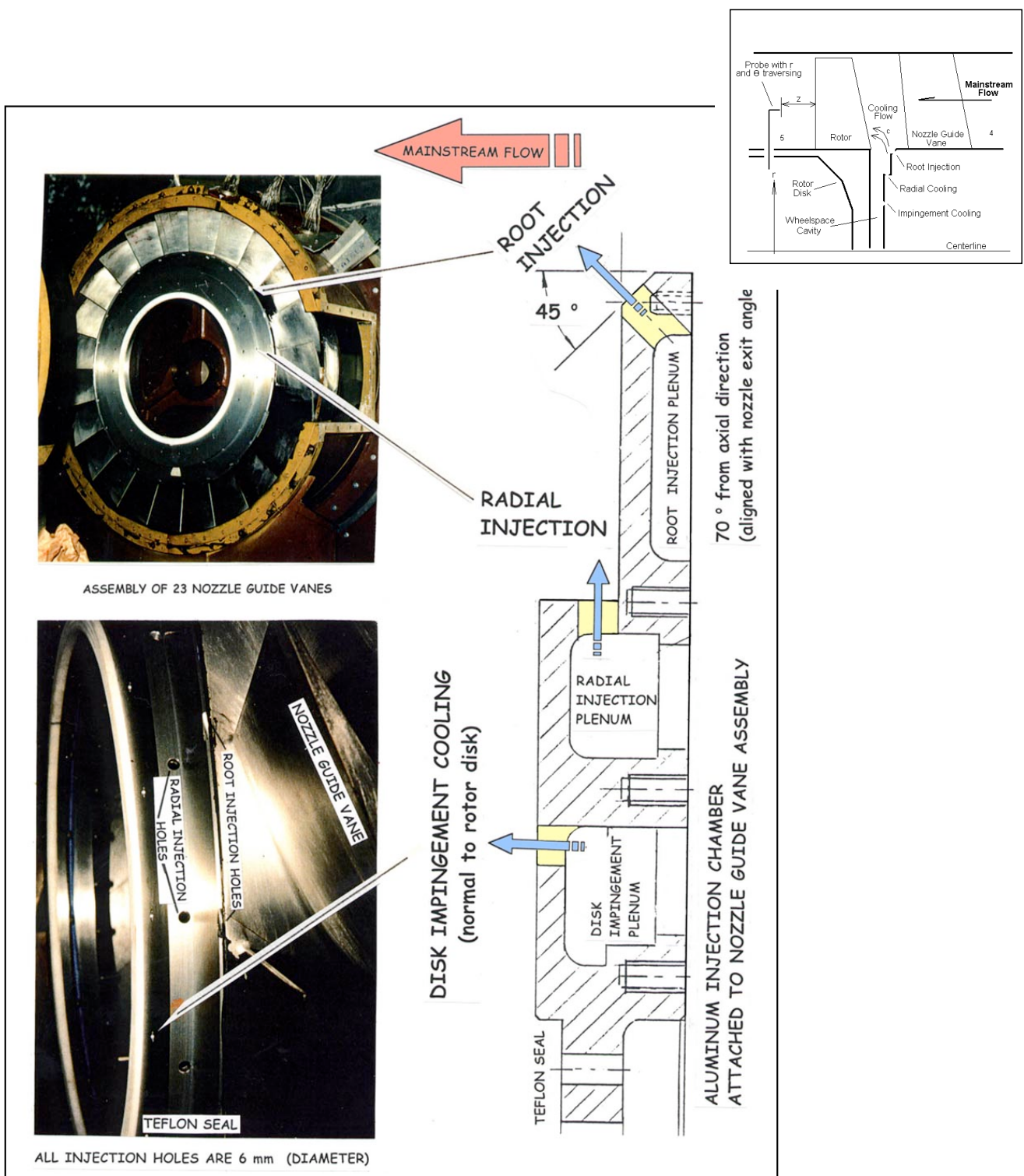


Figure 15. Intra-stage coolant injection system in AFTRF used by McLean&Camci [11], [12] (Disk impingement/Radial injection/Root injection) , © ASME

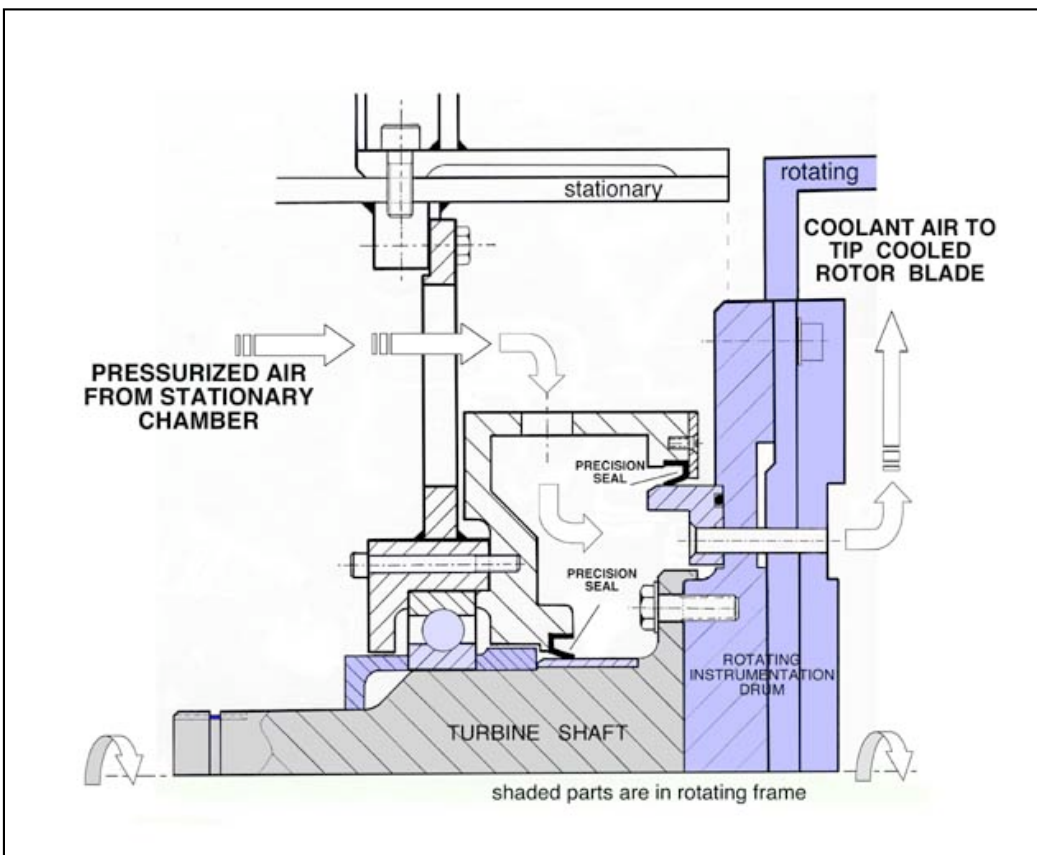
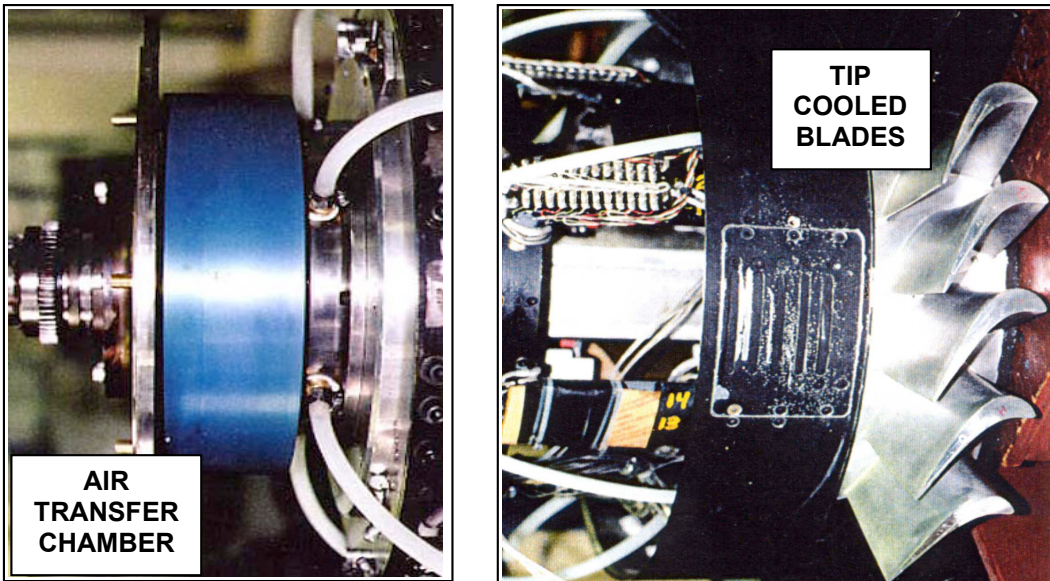


Figure 16. Air-transfer system used in tip cooling/de-sensitization studies in AFTRF
 Dey&Camci [13] , Rao&Camci [14], [15]
 (Tip cooled blades, top-right) , © ASME

Tip Cooling system: Figure 17 shows the current tip cooling arrangement designed and installed for the recent tip injection based tip desensitization studies in AFTRF. Discrete tip injection holes are shown inside a tip trench with a square cross section. The width and height of the tip trench is 0.030 inch. The approximately radially oriented plenum chambers are also shown in the inset. A detailed account of the aerodynamic de-sensitization effect of tip injection holes described in Figure 17 is given in Rao&Camci [14] and [15].

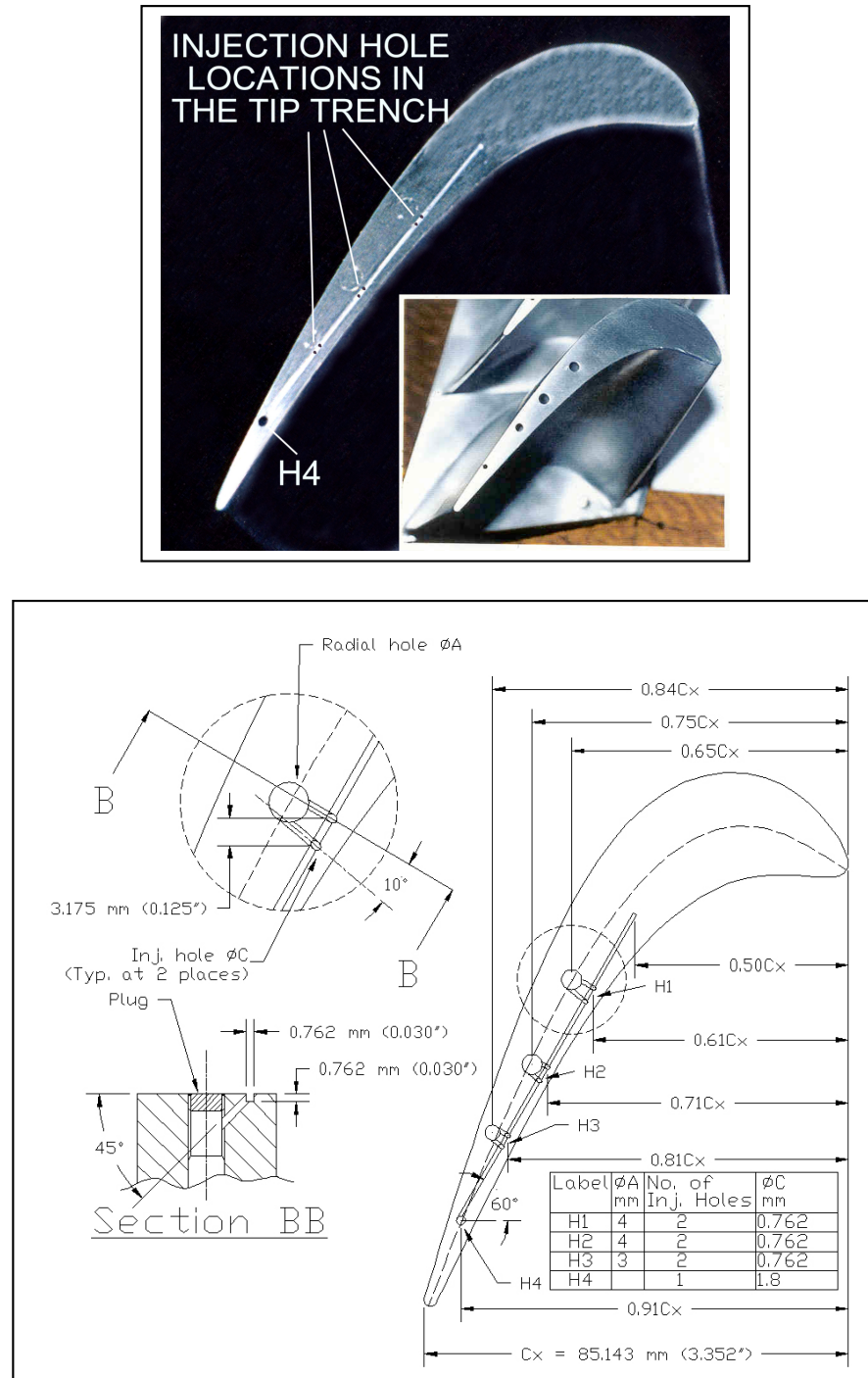
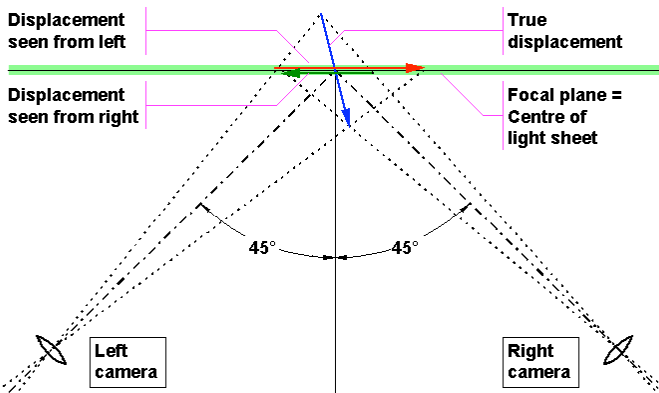


Figure 17. Tip cooling geometry used for tip de-sensitization studies in AFTRF by Rao&Camci [14]. [15]. ©ASME

Stereoscopic Particle Image Velocimeter in AFTRF: A particle image Velocimeter system is currently installed and fully operational in AFTRF. All three components of the velocity vector can be obtained after a phase-locked ensemble averaging procedure in turbine passages. Figure 18 shows the stereo vision principle used in the turbine 3D PIV measurements. The current system uses a horizontal laser light sheet passing from the axis of rotation of the turbine facility. The light sheet is generated by two 130 mJ pulsed Nd-Yag lasers. The two high-sensitivity cameras used could be either on one side of the light sheet as shown in Figure 18 or they could be located on both sides of the laser light sheet. A detailed explanation of the implementation details of this 3D PIV system are given in Tajiri [16].

Fundamentals of stereo vision



True 3D displacement ($\Delta X, \Delta Y, \Delta Z$) is estimated from a pair of 2D displacements ($\Delta x, \Delta y$) as seen from left and right camera respectively

Figure 18. The principle of stereoscopic vision (courtesy of Dantec Inc.)

Figure 19 is a sketch explaining a “double pulsed” laser sheet with a time separation as short as a few micro-seconds. Due to extremely short time separation between the two light sheet pulses, two individual Nd-Yag lasers are used in a double cavity mode as shown in the sketch. Each pulsed laser contributes to a green laser light sheet. The Nd-Yag lasers originally emit light at IR (infrared) wavelengths which is not visible. A frequency-doubler produces green light at a wavelength of 532 nm for visible laser sheet generation.

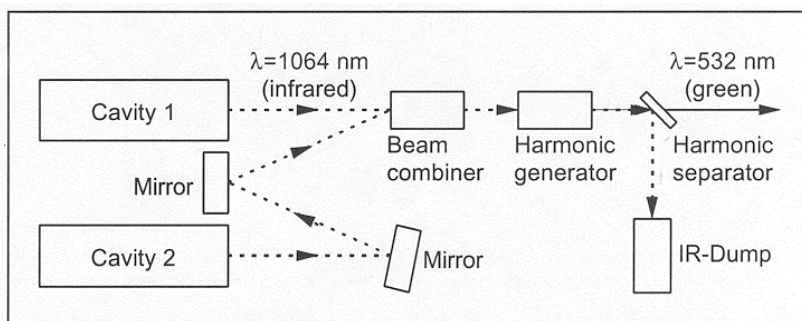


Figure 19. Generation of a double pulsed laser sheet from two individual 130 mJ Nd-Yag lasers operating in pulsed mode. (courtesy of Dantec Inc.)

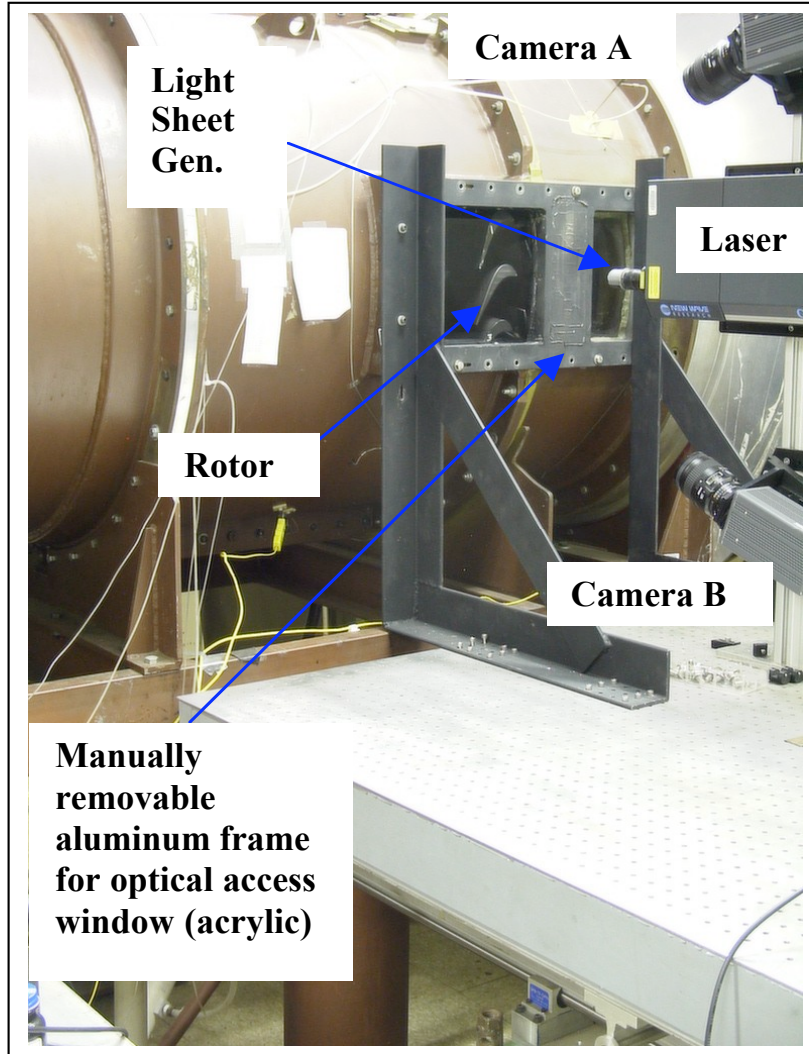


Figure 20, Stereoscopic PIV system installation in AFTRF from Tajiri [16].
The Nd-YAG laser, two high sensitivity cameras with Scheimpflug condition and the optical access window is visible.

3D PIV calibration in AFTRF: Figure 20 shows the installation details of the 3D PIV system in AFTRF. The laser sheet is horizontal and passes through the axis of rotation of the turbine. Current measurements are obtained for 11 consecutive positions of the turbine rotor. The two cameras and the laser head form a vertical plane normal to the axis of rotation. The camera optical axis in each camera is tilted with respect to the camera CCD normal axis in order to comply with the Scheimpflug condition imposed. The two cameras, the laser head, light sheet generator and the movable optical access window are attached to the same frame of reference. All of these components are attached to a precision made optical breadboard in a rigid fashion.. The optical breadboard could be moved away from the facility for calibration purposes. The details of the operation required for the proper calibration of the 3D PIV system including the optical influence of the curved access window are given in Tajiri [16].

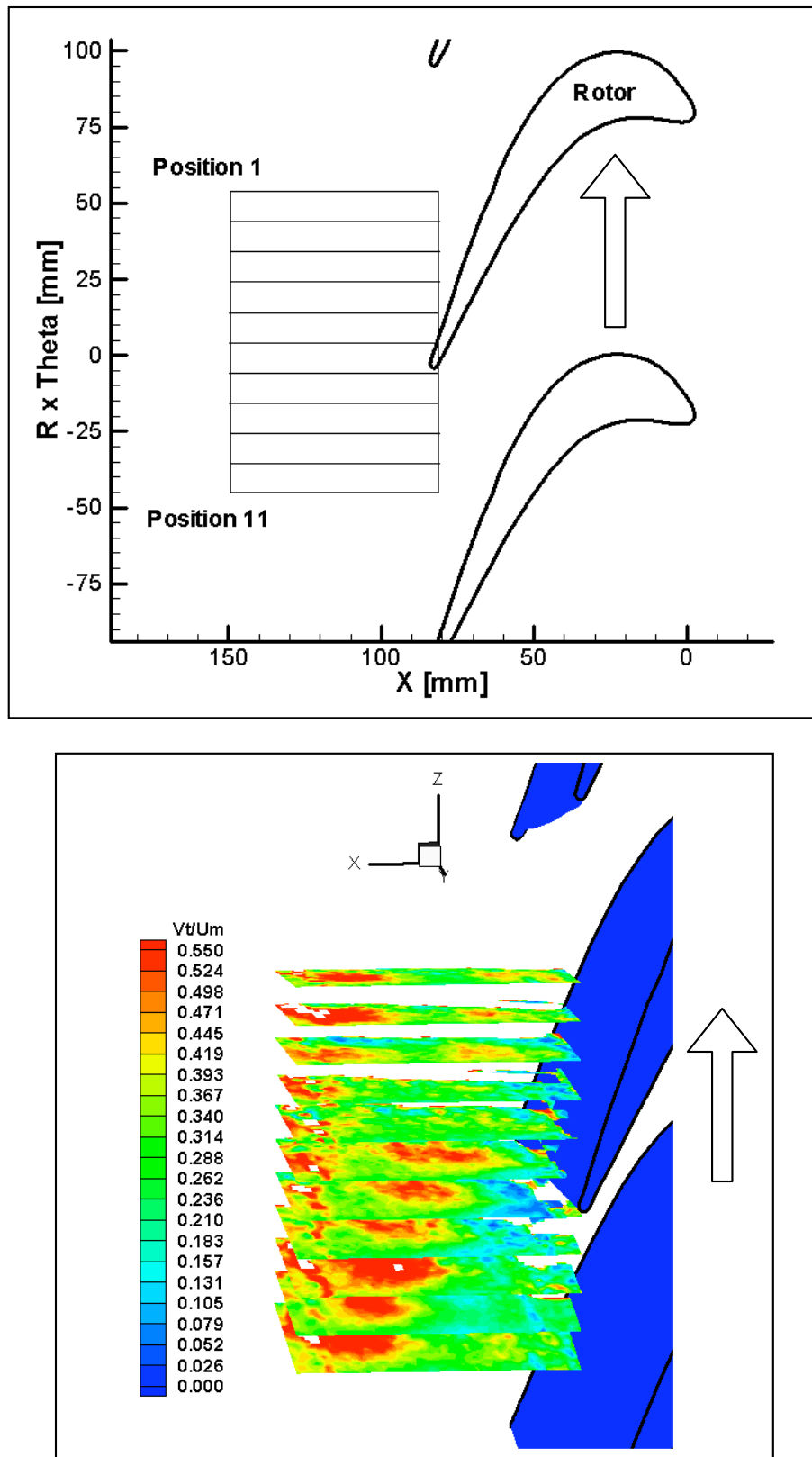


Figure 21. Stereoscopic PIV measurement planes downstream of the rotor and the magnitude of measured velocity (Phase-locked measurement for the shown position of the rotor.) from Tajiri [16].

CONCLUSIONS

The design, fabrication, assembly, shakedown and performance measurement of a state-of-the-art turbine research facility including the most recent modifications and developments are presented. The facility is equipped with an extensive set of instrumentation needed for the basic study of three dimensional unsteady and steady viscous flows in nozzle and blade rows, rotor-stator interaction, tip clearance and secondary vortex flows, as well as horseshoe vortex formation and transport of these vortices through the nozzle and blade rows. A general purpose cooling system for the rotor applications and intra-stage coolant injection system is fully operational. The facility has LDA and PIV systems as non-intrusive aerodynamic measurement systems. Conventional and sub-miniature aerodynamic probes, dynamic pressure transducers, wall shear stress sensors and various flow visualization methods are available. The facility is also currently equipped with a precision in-line torque measuring system for performance measurement purposes..

Acknowledgments

Although AFTRF was operational in early nineties, the facility was under constant modification over the last few years. The initial funding for this facility was provided by the Department of Defense through the Instrumentation Program (DAAL 03-86-G-OOI3), National Aeronautical Space Administration through the grant NAG 3-555 and The Pennsylvania State University. General Electric Company (Aircraft Engine Group) provided the design of blading and the flow path. A major facility such as this involves numerous organizations and individuals who contributed funds and assistance. Without their assistance the facility would not have been completed. These individuals are: T. Doligalski and RE. Singleton of the Army Research Office, K Civinskas, R Gaugler, L. Povinelli and J. Schwab of the NASA Lewis Research Center, D. Wisler and I.Halliwell of General Electric Co. Aircraft Engine Group. Some of the more recent modifications to the facility was supported by Solar Turbines Inc. and DOE/NETL/SCIES under AGTSR program. The continuous support from Drs.B.Glezer and E.Rajinsky of Solar Turbines is appreciated. The 3D PIV apparatus was funded by the DOD Army Research Office. The idea of developing and installing a turbine research rig at Penn State belongs to late Prof. Lakshminarayana.. The author is indebted to Prof. Lakshminarayana for his continuous criticism and suggestions over the years the AFTRF was developed into a fully operational turbine research facility.

References

- [1] Lakshminarayana, B., Camci, C., Halliwell, I., Zaccaria, M., 1996, "Design and Development of a Turbine Research Facility to Study Rotor-Stator Interaction Effects," Int.. Journal of Turbo and Jet Engines, Vol.13, pp.155-172.
- [2] Zaccaria, M. and Lakshminarayana, B., 1995, "Investigation of Three Dimensional Flow Field at the Exit of a Turbine Nozzle," AIAA Journal of Propulsion and Power, Vol.11, No.1, pp.55-63.
- [3] Smith, L.H., Jr., "The Radial Equilibrium Equation of Turbomachinery", 1966, ASME Journal of Engineering for Power, 88, pp. 1-12.
- [4] Wisler, D.C., 1985,"Loss Reduction in Axial Flow Compressors Through Low-speed Model Testing", ASME Journal of Eng. for Gas Turbines and Power, 107 (2), pp.354-362.
- [5] McCroskey, W.J., and Durbin, E.J., 1972, "Flow Angle and Shear Stress Measurements Using Heated Films and Wires", Transactions of the ASME, pp.46-52.
- [6] Lakshminarayana, B., 1981, "Techniques for Aerodynamic and Turbulence Measurements in Turbomachinery Rotors", J. Engineering for Power, 103 (2), pp.374-392.
- [7] Murthy, K.N.S., and Lakshminarayana, B., 1986, "Laser Doppler Velocimeter Measurements in the Tip Region of a Compressor Rotor", AIAA Journal, 24 (5), pp.807-814 .
- [8] Ristic, D., Lakshminarayana, B., Chu, S., 1998, "Three-dimensional Flow Field Downstream of an Axial Flow Turbine Rotor," AIAA paper 98-3572, presented at the 34th AIAA/ASME/SAE/ASEE Joint Propulsion Conference and Exhibit, Cleveland, Ohio.
- [9] Joslyn, D., and Dring, R, 1990, "Three-dimensional Flow in an Axial Turbine", ASME Paper 90-GT-56, 1990.

Nomenclature

C	Chord length
H	Blade height $\left(\frac{r - r_h}{r_t - r_h} \right)$
M	Mach number
N	Rotor speed RPM
p	Static pressure
Po	Stagnation pressure
R =	reaction = $\frac{\text{ideal static enthalpy drop across rotor}}{\text{ideal available energy across stage}}$ $= (h_{2a} - h_{3ss})/(h_{01} - h_{3ss})$
R	Radius (r/r_t)
Re	Reynolds number
r, θ, x	Radial, tangential and axial co-ordinates respectively
T_o	Stagnation temperature in °R
T_u	Turbulence intensity in the axial direction
U_m	Blade speed at mean radius
U_t	Blade tip speed
V	Absolute velocity
W	Relative velocity/weight flow - kg/sec
X	distance from leading edge
Δh_o	Decrease in enthalpy

$$\eta_s = \frac{\text{actual exit k.e.}}{\text{ideal exit k.e.}}$$

$$\eta_r = \frac{\text{actual relative exit k.e.}}{\text{ideal relative exit k.e.}}$$

$$\eta_{TT} = \frac{h_{01} - h_{03}}{h_{01} - h_{03s}}$$

Greek

γ	Meridional streamline angle measured from cylindrical surface in degrees
α	Absolute flow angle measured from axial direction in degrees
β	Relative flow angle measured from axial direction in degrees
θ, δ	$T/T_{SL}, P/P_{SL}$
ψ	Loading coefficient $2(P_{01}-P_{03})/\rho U_m^2$
ψ_s	Static pressure drop coefficient $2(p_1 - p_3)/\rho U_m^2$

Subscripts

1	Inlet to nozzle
2	Exit of nozzle
3	Exit of rotor

- [10] Boletis, E., and Sieverding, C.H., 1991, "Experimental Study of the Three-dimensional Flow Field in a Turbine Stator Preceded by a Full Stage", J. Turbomachinery, 113 (1), pp.1-9.
- [11] McLean., C. and Camci, C., 2001, "Mainstream Aerodynamic Effects due to Wheel Space Coolant Injection in a High Pressure Turbine Stage, **Part-1** Stationary Frame Measurements" ASME Journal of Turbomachinery, Vol.123, No.4, pp. 687-696.
- [12] McLean., C. and Camci, C., 2001, "Mainstream Aerodynamic Effects due to Wheel Space Coolant Injection in a High Pressure Turbine Stage, **Part-2** Rotational Frame Measurements" ASME Journal of Turbomachinery, Vol.123, No.4, pp. 697-703.
- [13] Dey, D. and Camci, C. 2000, "Development of Turbine Tip Clearance Flow Downstream of a Rotor Blade with Coolant Injection from a Tip Trench," Proceedings of the 8 th International Symposium on Transport Phenomena and Dynamics of Rotating Machinery (ISROMAC-8), pp.572-579.
- [14] Rao, N. and Camci, C., 2004, "Axial Turbine Tip De-sensitization by Injection From a Tip Trench, **Part-1** Effect of Injection Mass Flow Rate" ASME Paper GT2004-53256.
- [15] Rao, N. and Camci, C., 2004, "Axial Turbine Tip De-sensitization by Injection From a Tip Trench, **Part-2** Leakage Flow Sensitivity to Injection Location" ASME Paper GT2004-53256.